

Magnetic phase evolution in the spinel compounds $\text{Zn}_{1-x}\text{Co}_x\text{Cr}_2\text{O}_4$

Brent C. Melot, Jennifer E. Drewes, and Ram Seshadri

Materials Department and Department of Chemistry and Biochemistry
University of California, Santa Barbara CA 93106

E-mail: bmelot@mrl.ucsb.edu, jennidrewes@umail.ucsb.edu, seshadri@mrl.ucsb.edu

E. M. Stoudenmire

Department of Physics
University of California, Santa Barbara CA 93106

E-mail: miles@physics.ucsb.edu

Arthur P. Ramirez

LGS, 15 Vreeland Road, Florham Park, New Jersey NJ 07932

E-mail: apr@LGSInnovations.com

Abstract.

We present the magnetic properties of complete solid solutions of ZnCr_2O_4 and CoCr_2O_4 : two well-studied oxide spinels with very different magnetic ground states. ZnCr_2O_4 , with non-magnetic d^{10} cations occupying the A site and magnetic d^3 cations on the B site, is a highly frustrated antiferromagnet. CoCr_2O_4 , with magnetic d^7 cations (three unpaired electrons) on the A site as well, exhibits both Néel ferrimagnetism as well as commensurate and incommensurate non-collinear magnetic order. More recently, CoCr_2O_4 has been studied extensively for its polar behavior which arises from conical magnetic ordering. Gradually introducing magnetism on the A site of ZnCr_2O_4 results in a transition from frustrated antiferromagnetism to glassy magnetism at low concentrations of Co, and eventually to ferrimagnetic and conical ground states at higher concentrations. Real-space Monte-Carlo simulations of the magnetic susceptibility suggest that the first magnetic ordering transition and features of the susceptibility across x are captured by near-neighbor self- and cross-couplings between the magnetic A and B atoms. We present as a part of this study, a method for displaying the temperature dependence of magnetic susceptibility in a manner which helps distinguish between compounds possessing purely antiferromagnetic interactions from compounds where other kinds of ordering are present.

PACS numbers: 75.30.Kz 75.50.Ee 75.50.Gg

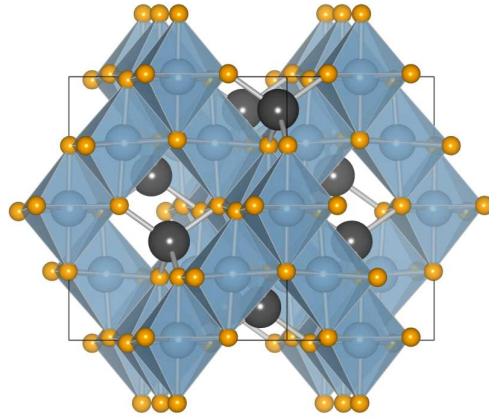


Figure 1. (Color online) Spinel AB_2O_4 structure showing edge-shared laths of BO_6 octahedra (blue-grey) with B–B magnetic coupling across the edges. Tetrahedrally coordinated A atoms (dark grey) connect the octahedral laths, and each A atoms has four B near-neighbors. Oxygen are orange.

1. Introduction

Geometrically frustrated spin systems[1] have been extensively investigated because of the fascinating fundamental physics they display. More recently, they have attracted interest due to their frequently possessing ground states with spiral magnetic structures.[2] Recent interest in such structures has been engendered by the rediscovery of systems where the magnetic ordering does not have a center of symmetry, and there is perforce a loss of a center of symmetry in the crystal structure as well. This helps to couple lattice and spin degrees of freedom and gives rise to a plethora of magnetoelectric phenomena.[3, 4, 5, 6, 7, 8, 9, 12, 13]

The spinel structure type (displayed in figure 1) with the general formula AB_2X_4 , has been extensively studied in this light because of its ability to host magnetic cations on both its tetrahedrally coordinated A sublattice as well as its octahedrally coordinated B sublattice. Additionally, both sublattices are geometrically frustrated with octahedral B sites forming a pyrochlore network, and the tetrahedral sites forming a diamond lattice. The former intrinsically displays geometric magnetic frustration associated with the difficulty of decorating the vertices of a tetrahedra with spins that are antialigned. The latter is frustrated because of competing near- and next-near neighbor interactions.[14, 15, 16]

Conventional wisdom, however, is that the dominant magnetic interactions are between the A and the B sublattices provided there are magnetic ions on both sites. Adding to the complex nature of magnetic interactions in the spinel structure is that superexchange interactions between A-sites are mediated by atoms on the B-site (even when the B site is non-magnetic), and in the same vein, B-B next-nearest-neighbor interactions are mediated by the A site ion.[17] In the cubic spinel, the

number of near neighbors (NN) and next-near-neighbors (NNN) for A are 4A(NN), 12B(NN), 12A(NNN), and 16B(NNN). For B, the distribution is 6A(NN), 6B(NN), 8A(NNN), and 12B(NNN). In addition, most of the coupling pathways are multiply degenerate. These result in next-near neighbors contributing in an important manner to the overall magnetic ordering behavior.[14, 15] The high connectivity of the spinel lattice has been shown to give rise to a vast array of interesting magnetic phenomenon. [9, 8, 13, 18, 19, 20, 21, 22, 23]

Chromium spinels, where the B sublattice is fully occupied by Cr^{3+} , present a unique opportunity to examine these complex magnetic interactions due to the fact that Cr^{3+} will not invert to the tetrahedral A sites unlike many other transition metals, as a result of the very strong crystal field stabilization of octahedral d^3 cation (t_{2g}^3 crystal field). Here we prepare and study clean samples of solid solutions of $ZnCr_2O_4$ and $CoCr_2O_4$, two well studied chromium spinels with very different magnetic ground states. $ZnCr_2O_4$, with a non-magnetic cation occupying the A site, undergoes a spin-driven Jahn-Teller-like distortion at low temperatures which results in a Néel-type antiferromagnetic order.[24, 25] $CoCr_2O_4$, with magnetic cations on both sublattices, displays collinear ferrimagnetic as well as non-collinear spiral magnetic ordering.[26] By replacing the Zn with Co our goal is to introduce magnetic interactions into an otherwise non-magnetic lattice and observe the effect this would have on the magnetic frustration of the system. This series is particularly interesting because it provides the opportunity to study the effects of dilute magnetic interactions in the absence of changes to the superexchange angle (Co^{2+} and Zn^{2+} have very similar ionic radii) or site disorder (because of the strong octahedral site preference of Cr^{3+}). We find for low concentrations of Co, a seeming increase in frustration resulting from spin disorder which results in a glassy magnetic state. At higher Co concentrations there is evidence that the spins form non-collinear structures reminiscent of the $CoCr_2O_4$ end member.

Monte Carlo simulations of Heisenberg spin systems have been performed which allow comparisons with the experimental magnetic susceptibility, and yield the appropriate range of J couplings between the different sites to be estimated. They also suggest the minimal models required to describe the gross aspects of the magnetic susceptibility in these systems. We also demonstrate here that appropriate scaling of Curie-Weiss plots of the inverse magnetic susceptibility as a function of temperature allows for systems with purely antiferromagnetic interactions to be distinguished by systems with more complex interactions.

2. Experimental details

Polycrystalline samples in the series were prepared by solid state routes. Appropriate stoichiometric amounts of cobalt oxalate ($CoC_2O_4 \cdot 2H_2O$), ZnO, and Cr_2O_3 were mixed and ground with ethanol in an agate mortar. The powders were then pressed into 13mm pellets and calcined in alumina crucibles at 800°C for 12h. These pellets were then reground, pressed back into pellets, and fired at 1150°C for 12h. The pellets were

then briefly annealed at 800°C for 24 h. During all heatings, the pellets were placed on a bed of powder with the same stoichiometry to minimize reaction with the crucible. X-ray diffraction patterns were obtained using Cu-K α radiation on a Philips XPERT MPD diffractometer operated at 45 kV and 40 mA. Phase purity was subsequently determined by refining the patterns using the Rietveld method as implemented in the XND Rietveld code.[27] DC magnetization measurements were carried out using a Quantum Design SQUID magnetometer.

3. Computational Details

Classical Monte Carlo simulations of the magnetic behavior of the system were performed using the ALPS project’s SPINMC application [28]. We generated a lattice with the appropriate fraction of A sites occupied for each simulation run in order to perform disorder averaging. The magnetic interactions were modeled by a nearest-neighbor Heisenberg Hamiltonian with antiferromagnetic couplings J_{BB} , J_{AB} and J_{AA} where the subscripts specify the sublattice types of the two spins connected by a given interaction. Since the number of J_{BB} interactions in the system does not vary with x , the other two couplings are varied relative to J_{BB} , which is set to unity (in Monte-Carlo units) throughout.

The inverse magnetic susceptibility of each simulated system was fit to the experimental data by scaling both sets of data such that they satisfy the Curie-Weiss relationship at high temperature. This is the same method used to plot the experimental data described below – see equation (3). It should be noted, however, that in these simulations, “high temperature” means high relative to the temperature at which the inverse susceptibility strongly deviates from linear behavior. As discussed in what follows, the experiments could not actually be performed above $T = |\Theta_{CW}|$ where the Curie-Weiss law is strictly applicable. Numerical simulations could indeed verify the following analytic expression for the Curie-Weiss temperature of the nearest-neighbor model

$$\Theta_{CW} = \frac{-2S(S+1)}{3(1+\frac{x}{2})}(3J_{BB} + 6xJ_{AB} + x^2J_{AA}) \quad (1)$$

After a reasonable fit to the susceptibility was found for each experimental dataset, corresponding to the different x values, the simulations were run again using a newly generated random lattice as many as 3 times to determine the effect of disorder. A disorder average was then performed by averaging the resulting inverse susceptibilities and the disorder error bars were taken to be the standard deviation of this average. Finally, it should be noted that since the simulations were run until the Monte Carlo error was negligible (relative errors of about 10^{-4}), all numerical error bars shown below represent only the disorder error bars with the exception of the disorder-free $x = 1.0$ end member.

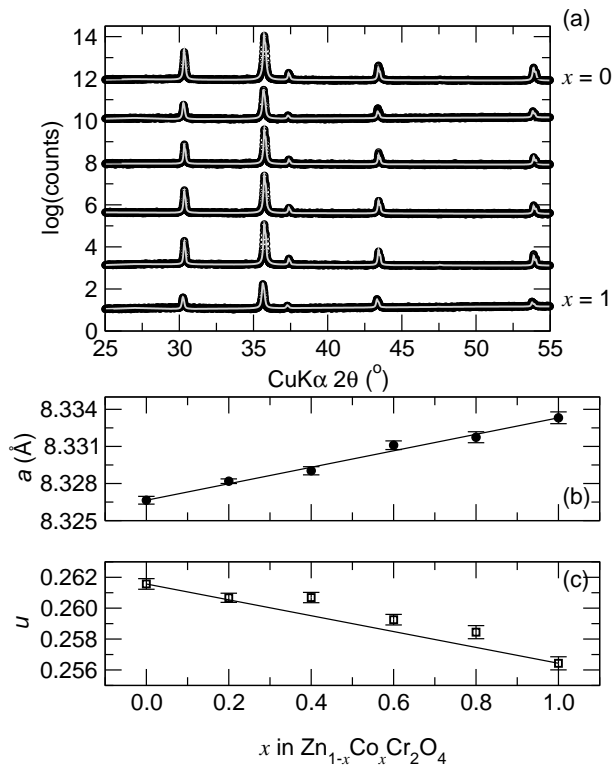


Figure 2. A portion of the room temperature x-ray diffraction patterns of $\text{Zn}_{1-x}\text{Co}_x\text{Cr}_2\text{O}_4$. (a) Points are data and solid grey lines represent the Rietveld least-squares analysis. (b) Evolution of the cubic cell parameter with Co content x . The line connecting end members is drawn as a guide to the eye to illustrate the Végard law. (c) Shows the steady decrease with x of the internal positional parameter u of oxygen.

4. Results and Discussion

A portion of the X-ray diffraction patterns of the solid solution series are presented in figure 2. All samples were found to be single phase with no extraneous peaks. The patterns were fit using the Rietveld method to the normal cubic spinel crystal structure with appropriate mixed occupancies on the A site. The cubic cell parameter and the position of the oxygen atom (u, u, u) in the unit cell were obtained from the refinement. Because Co and Zn are relatively similar in terms of their x-ray scattering powers, no attempt was made to extract the relative concentrations of these ions in the lattice.

The cell parameter a and oxygen position u extracted from the Rietveld refinements are presented in figure 2(b) and (c). Co^{2+} and Zn^{2+} in tetrahedral coordination have very similar ionic radii, 0.58 Å and 0.60 Å respectively,[29] with Co^{2+} the slightly smaller ion. Increasing Co in the compounds should therefore lead to a contraction of the cell parameter. We find, however, a small expansion of the unit cell volume. This is consistent with previously reported structures of the end members.[30] A possible reason for the expansion is that tetrahedral Co^{2+} is more ionic than Zn^{2+} and the substitution of Zn by Co introduces A–B cation-cation repulsions which expand the lattice. Expansion

Table 1. Results from fitting the inverse magnetic susceptibility data to the Curie-Weiss equation. Θ_{CW} is taken as the x -intercept of the inverse susceptibility curve while T_c is chosen as the first point of inflection in the first derivative of the susceptibility with respect to temperature. f is defined as the absolute ratio of Θ_{CW} to T_c . The experimental effective moment is calculated using the relation $\mu_{\text{eff}}^2 = 3Ck_B/N$ where C is the slope of the inverse susceptibility versus temperature. The estimated moments (spin-only, and unquenched) are obtained using $\mu_{\text{eff}} = \sqrt{\mu_{\text{Co}}^2 + 2\mu_{\text{Cr}}^2}$.

	$\mu_{\text{eff}} (\mu_B)$			Θ_{CW} (K)	T_c (K)	f
	measured	spin-only	unquenched			
ZnCr ₂ O ₄	5.2	5.5	5.5	-298	19	16
$x = 0.2$	5.7	5.8	6.0	-380	8	51
$x = 0.4$	6.0	6.0	6.4	-424	15	28
$x = 0.6$	6.9	6.3	6.8	-592	20	30
$x = 0.8$	6.7	6.5	7.2	-488	55	9
CoCr ₂ O ₄	7.5	6.7	7.6	-568	75	8

in the cell parameters in order to minimize repulsion between neighboring cations has been suggested in other spinel systems.[31]

Changes in the u parameter associated with O atoms in the unit cell occur as the structure tries to accommodate cations of different sizes. When $u = 0.25$, the anions are in an ideal cubic-close-packed arrangement, with perfect CrO₆ octahedra, while values of $u > 0.25$ indicate an increase in size of the tetrahedron with a corresponding shrinkage and trigonal compression of the octahedron.[30] As seen from figure 2(c), there is a systematic decrease in u with x which brings it closer to the ideal value. This decrease implies that the tetrahedral sites shrink across the series, in keeping with the smaller size of Co²⁺, but in contradiction with the unit cell expansion.

The high temperature (200 K to 300 K) susceptibility of the samples was fit to the Curie-Weiss equation, $\chi = C/(\chi - \Theta_{CW})$, to obtain the effective paramagnetic moment μ_{eff} from the Curie constant C , and the Curie-Weiss intercept Θ_{CW} . These values are presented in table 1. The orbital-quenched, spin-only effective moment ($\mu_S = 2\sqrt{S(S+1)}$) for free ions of both Co²⁺ and Cr³⁺ is $3.88 \mu_B$. Figure 3 shows an increase in the experimental μ_{eff} with increasing values of x . It is noted that samples with $x \leq 0.4$ agree well with the spin-only moment. $x \geq 0.6$ is anomalous in terms of the trend with x . The $x = 0.8$ and $x = 1.0$ samples tend increasingly to an effective moment value that is closer to the value expected for the unquenched orbital contribution from Co²⁺, $\mu_S = \sqrt{4S(S+1) + L(L+1)}$. While this may be unexpected for Co²⁺ in a tetrahedral coordination environment which has no orbital degeneracy, the presence of the low lying ($e^3t_2^4$) excited state could be a source for this increased moment.[32] Cr³⁺ is expected to remain strongly orbital quenched. The change from orbital quenched (spin-only) to unquenched behavior for Co²⁺ in this system may have to do with the small changes in structure as x is increased.

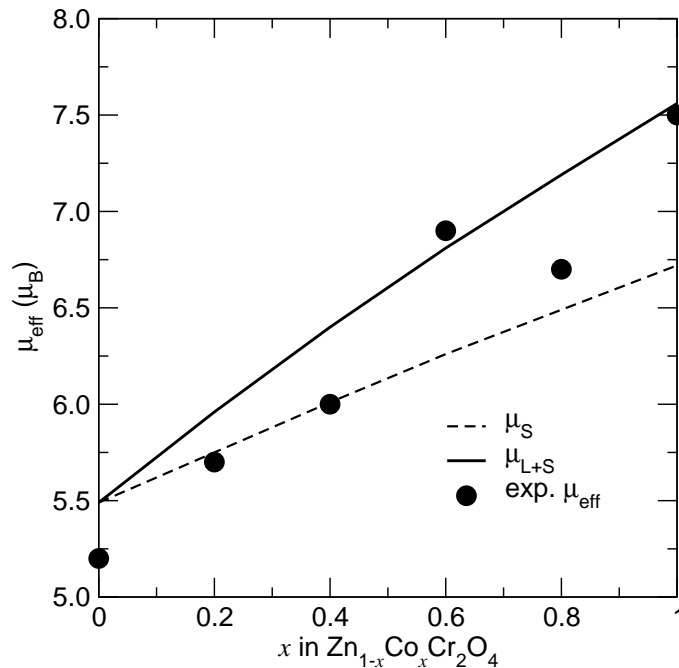


Figure 3. Effective magnetic moment obtained from the Curie-Weiss fit to the high temperature inverse susceptibility data for $\text{Zn}_{1-x}\text{Co}_x\text{Cr}_2\text{O}_4$. The two lines represent the expected values calculated for a fully quenched (μ_S) Co^{2+} and Cr^{3+} , and a fully unquenched (μ_{L+S}) Co^{2+} orbital contribution to the magnetic moment.

It was recently suggested that the introduction of magnetic cations into ZnCr_2O_4 has the effect of introducing short range order in the high temperature paramagnetic regime,[33] and this can be a source of the small underestimation observed here. In addition, even in dilute spinel systems with Cr^{3+} , near-neighbor coupling effects are known,[34] and such coupling can invalidate the assumption made here of independent spins. We note, however, that the effective moment we have determined for ZnCr_2O_4 falls within the range of previously reported values [10, 11] which vary from 5.1-5.6 μ_B f.u.⁻¹. We were unable to find any previous reports for the effective moment of CoCr_2O_4 .

As x increases, so do the magnitudes of the Curie-Weiss Θ_{CW} , reflecting the increasing numbers of the dominant antiferromagnetic A-B interactions. The increase is monotonic with the exception of $x = 0.6$, which seem anomalous in this series.

Figure 4 illustrates the temperature dependence of the DC magnetization with the response of the end members in good agreement with previously reported data.[24, 26] The sharp drop in the susceptibility of ZnCr_2O_4 is characteristic of the spin-driven Jahn-Teller distortion that allows the system to order in a Néel-type antiferromagnetic ground state.[24] Dilute concentrations of Co result in this sharp drop being lost, which indicates the structural distortion is likely suppressed and instead the characteristic behavior is of spins freezing into a glassy state. For concentrations of Co above 60%, Néel-type ferrimagnetism is stabilized. The highest ordering temperatures T_c for the different compounds are also listed in table 1, obtained by taking the first derivative of the susceptibility with respect to temperature. The frustration index $f = \Theta_{CW}/T_c$

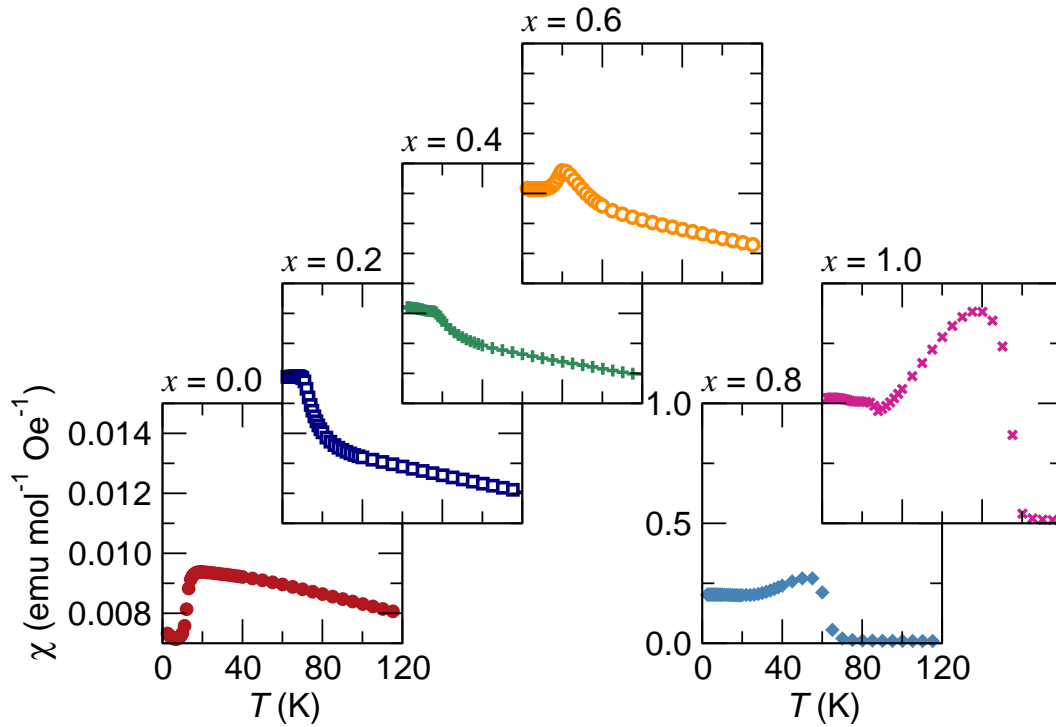


Figure 4. (Color online) Field cooling curves were collected under a static DC field of 1000 Oe. Pure ZnCr_2O_4 sample orders antiferromagnetically below its Néel temperature while samples with $0 < x \leq 0.6$ exhibit glassy behavior resulting from the dilute uncompensated antiferromagnetic interactions because of A–B interactions between Co^{2+} and Cr^{3+} . Samples with $x = 0.8$ and $x = 1.0$ order ferrimagnetically below their highest transition temperature, and then transform to more complex orderings.

is listed in the last column of the table. It is seen that all the compounds order at temperatures much lower than would be otherwise expected, *ie.* all the compounds in the series are frustrated. The initial increase in the frustration index with x arises because of quenched disorder introduced by some of the A-sites having magnetic moments, and is not a true measure of geometric frustration.

We can rearrange the Curie-Weiss equation:

$$\chi = \frac{C}{T - \Theta_{CW}} \quad (2)$$

in the following manner:

$$\frac{C}{\chi\Theta_{CW}} = \frac{T}{\Theta_{CW}} - 1 \quad (3)$$

A plot of $C/(\chi|\Theta_{CW}|) - 1$ as a function of $T/|\Theta_{CW}|$ collapses all the high temperature susceptibility data in the manner displayed in figure 5. The straight line through the origin corresponds to ideal Curie-Weiss behavior and can be used as a measure of the quality of the fits in the high temperature regime. It is evident once again that all magnetic ordering takes place at temperatures much smaller than $T = \Theta_{CW}$ suggesting

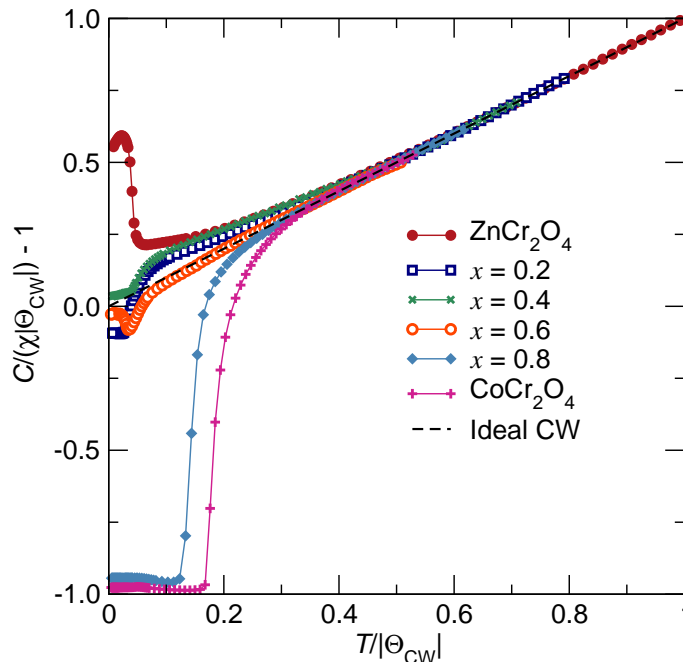


Figure 5. (Color online) Scaled inverse susceptibility as a function of scaled temperature, as described by the formula in 3. The dashed line represents ideal Curie-Weiss paramagnetism. Positive deviations from this line reflect the presence of compensated antiferromagnetic interactions, while negative deviations reflect uncompensated interactions and a tendency to ferrimagnetic ground states.

frustration. (Note the horizontal axis in this plot is an inverse of the frustration index f .) The modified Curie-Weiss plot displayed in figure 5 also quickly allows one to distinguish the nature of the dominant magnetic exchange interactions. Positive deviations from the ideal Curie-Weiss line (dashed) correspond to samples with purely compensated antiferromagnetic interactions. Even small amounts of Co^{2+} on the A site result in uncompensated antiferromagnetism (ferrimagnetism) and this manifests as negative deviations from the ideal line. As larger amounts of Co^{2+} are substituted, this residual paramagnetism is lost and the ground states resemble partially saturated ferrimagnets.

The modified Curie-Weiss plot depicted in figure 5 superficially resembles a semilog plot of resistivity *versus* temperature for a series of samples undergoing (typically) a composition driven metal-insulator transition. The line or curve separating insulators from metals is almost horizontal and frequently extrapolates, at 0K, to the inverse of the Mott minimum metallic conductivity.[35, 36] Insulators (localized systems) lie above this line, and metals (extended systems) lie below. In the same vein, samples in the series considered here show (appropriately scaled) inverse susceptibilities which lie above the Curie-Weiss line provided all interactions are antiferromagnetic and fully compensated, and these are distinct from samples with uncompensated interactions or with ferromagnetic interactions which are analogues of extended states. Analogies with thermal expansion can be drawn as well. Localized (Einstein) modes can decrease thermal expansion coefficients in crystals, and even make it negative. Extended

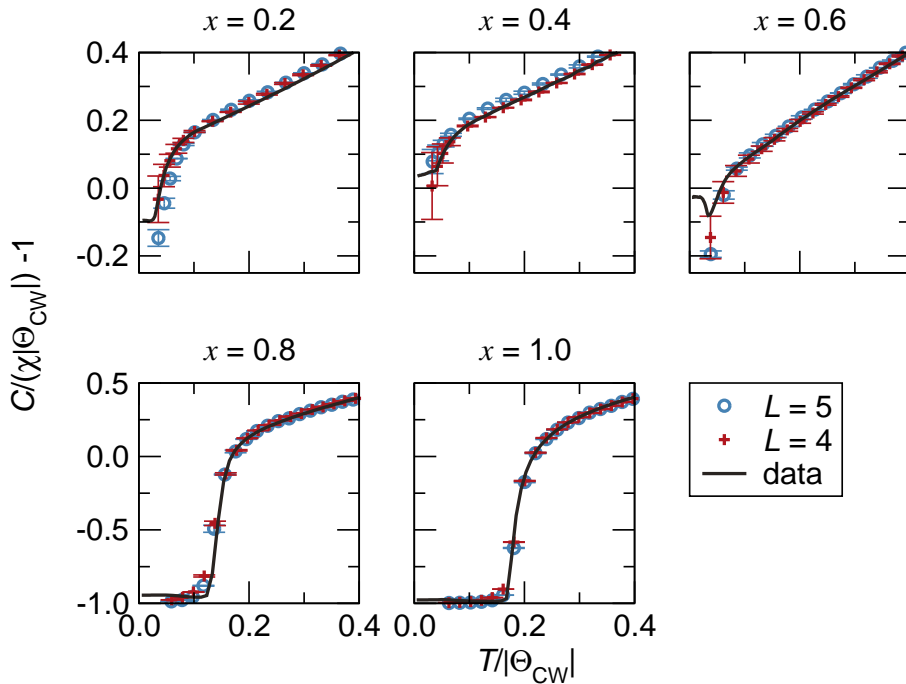


Figure 6. Comparison of the experimental magnetic susceptibilities with Monte Carlo simulations performed for the corresponding x values using the J couplings listed in table 2. L corresponds to the system size used in the simulation.

Table 2. Estimates of the Heisenberg coupling constants that best describe the experimental data. The J_{BB} estimates were obtained by solving equation 1 for J_{BB} using the Θ_{CW} estimates in table 1. The range of J_{BB} values for $x = 0.2$ corresponds to a J_{AA}/J_{BB} between 0.0 and 0.5.

	J_{AA}/J_{BB}		J_{AB}/J_{BB}		$J_{BB}(K)$
	estimate	error	estimate	error	
ZnCr ₂ O ₄	-	-	-	-	-
$x = 0.2$	(no dependence)		0.800	0.025	42.0-42.3
$x = 0.4$	0.3	0.1	0.775	0.025	41.5
$x = 0.6$	0.5	0.2	0.377	0.003	67.9
$x = 0.8$	0.4	0.1	0.930	0.02	35.4
CoCr ₂ O ₄	0.55	0.05	1.02	0.01	35.2

modes (Debye) usually give rise to the more common positive coefficients of thermal expansion.[37]

It turns out that a simple quantitative understanding of the susceptibility data in figure 5 is possible as well. We performed classical Monte Carlo simulations of the nearest-neighbor Heisenberg model on a B site spinel with A site doping and found a series of Heisenberg coupling parameters J_{AA}/J_{BB} and J_{AB}/J_{BB} that bring the simulations into rather close agreement with the experimental susceptibility

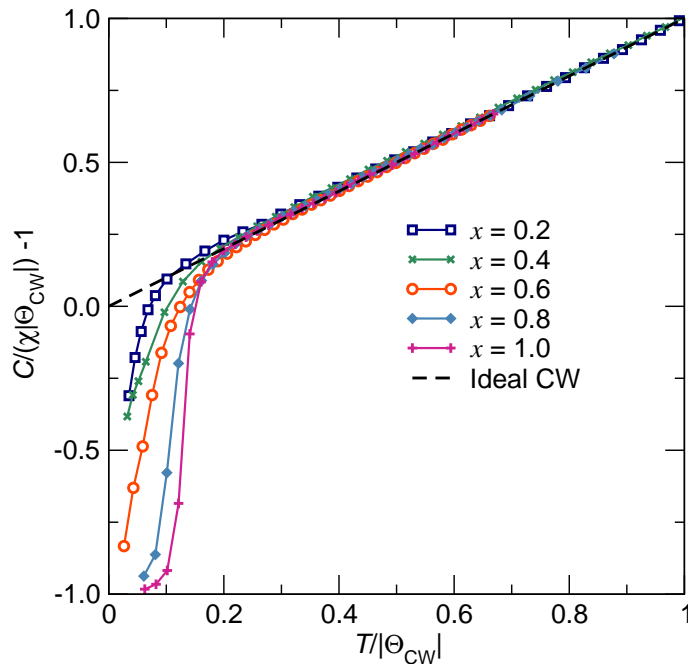


Figure 7. Results of Monte Carlo simulations on Heisenberg spin systems with a system size of $L = 4$ and the following coupling parameters: $J_{AA}/J_{BB} = 0.45$ and $J_{AB}/J_{BB} = 0.90$.

measurements.

The best fits obtained are shown in figure 6 and the resulting coupling constant estimates are summarized in table 2. The fits were first found using systems consisting of 4^3 conventional cubic unit cells (1024 B sites) with periodic boundary conditions. We then checked the finite-size scaling on systems of 5^3 unit cells (2000 B sites). It should also be noted that these best fits were determined by searching the parameter space, not by an optimization algorithm, so that quite likely even better agreement is possible using the same model.

We were encouraged to see that all of the best J_{AA}/J_{BB} and J_{AB}/J_{BB} parameters do not differ much from each other (the $x = 0.2$ data had too weak a dependence on J_{AA} for us to determine it effectively). Evidently, the bulk magnetic behavior of the entire series of materials is well described by taking J_{AB} to be comparable to J_{BB} and taking J_{AA} to be about half of J_{BB} . Accordingly, it was considered useful to actually fix all the couplings to such values and only vary x – the resulting scan (see figure 7) shows that it is indeed the value of x that most strongly determines the bulk magnetic properties of the system. The surprise is that for the range of parameters studied by which seem to be close to the experimentally measured susceptibility, J_{AB} and J_{BB} are effectively equal, rather than J_{AB} being significantly larger than J_{BB} ; the frequent expectation. Lyons, Kaplan, Dwight, and Menyuk (LKDM) [38] have proposed the following inequality: $(4J_{BB}S_B)/3J_{AB}S_A \leq 8/9$ implies collinear Néel ordering of moments in spinels such as CoCr_2O_4 . For $(4J_{BB}S_B)/3J_{AB}S_A > 8/9$ non-collinear ordering is suggested. Since in CoCr_2O_4 , $S_A = S_B$, we expect that if $J_{BB} \approx J_{AB}$, the ground state will be non-collinear,

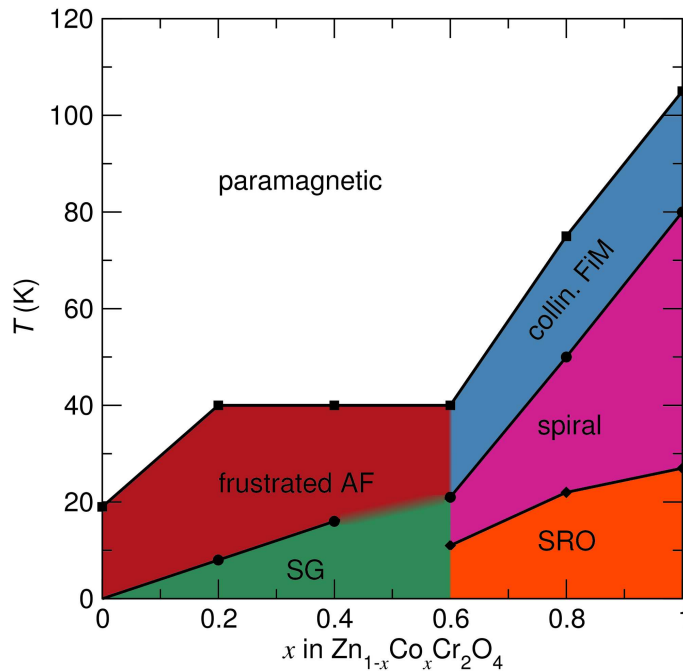


Figure 8. Tentative magnetic phase diagram as a function of Co content and temperature. Low concentrations of Co results in a glassy freezing of the spins at low temperature while higher concentrations drive the system to order in a non-collinear spiral structure. The points in the diagram correspond to changes of slope in the susceptibility as a function of temperature. (SG = spin glass, AF = antiferromagnetism, FiM = ferrimagnetism, SRO = short range ordering)

which is certainly true for $CoCr_2O_4$. So the Monte Carlo estimates of J_{BB} and J_{AB} are consistent with the experimental realization of non-collinear ground states.[26] Recently Ederer and Komeilj[39] have performed detailed density functional calculations on the $x = 1$ end-member, $CoCr_2O_4$. They suggest that J_{AA} is important (ignored by LKDM) as determined here as well. While J_{AA} in their calculations is determined to be typically less than J_{BB} , they estimate that J_{AB} can be even twice as large as J_{BB} which is not the result obtained in the preliminary analysis presented here.

The results of the field-cooled susceptibility traces was used to construct a tentative magnetic phase diagram for the solid solutions as depicted in figure 8. We use changes in the slope of the field-cooled susceptibility as a function of temperature to obtain the boundaries between different magnetic phases. Regardless of composition, all samples demonstrate paramagnetic behavior at high temperatures and begin to show transitions to long range order starting near 100 K. The end member $ZnCr_2O_4$ is the only compound which exhibits long range antiferromagnetic order because of its structural distortion. We make the reasonable assumption that even small amounts of Co result in glassy behavior as indicated by the line separating frustrated antiferromagnetism from glassy states. For concentrations of $x \geq 0.6$ the magnetic behavior begins to look more like that of $CoCr_2O_4$ with a collinear ferrimagnetic transition between 50 K and 100 K followed by a transition into a non-collinear spiral at lower temperatures. The behavior near x

= 0.6 is rather complex and more experiments will be particularly important for this region of the phase diagram. The transition temperatures for the spiral appear to be slightly suppressed by Zn substitution with respect to the end member as illustrated by the positive slope of the phase boundary as the $CoCr_2O_4$ end member is approached. For the Co-rich compounds at the lowest temperatures, the structures begin to develop some spiral short range order (SRO).[26]

In summary, we have prepared and studied the magnetic properties of a solid solution of $ZnCr_2O_4$ and $CoCr_2O_4$. We have found that replacing non-magnetic cations with magnetic cations in the tetrahedral sites of a well ordered spinel results in a transition from glassy behavior at low concentrations of magnetic cations into a Néel-like ferrimagnetic order as well as commensurate and incommensurate magnetic spirals. These results are significant because they demonstrate that the presence of magnetic cations on the A-site can have the effect of relieving magnetic frustration on the B-site by allowing the system to find a lower energy state in the form of non-collinear magnetic spirals. Monte Carlo simulations suggest the minimum physics required to describe trends in the magnetic behavior, and suggest the range of strengths of the different magnetic couplings. We also present a useful form for plotting susceptibility data as a function of temperature which allows us to easily recognize the existence of uncompensated magnetic interactions in otherwise antiferromagnetic systems.

5. Acknowledgements

EMS would like to acknowledge encouraging discussions with Leon Balents. The National Science Foundation for support through a Career Award (NSF-DMR 0449354), and for the use of MRSEC facilities (Award NSF-DMR 0520415). JED was supported by the RISE program at the UCSB MRL.

- [1] Ramirez A P 1994 *Annu. Rev. Mater. Sci.* **24** 453
- [2] Kimura T 2007 *Annu. Rev. Mater. Res.* **37** 387
- [3] Kimura T, Goto T, Shintani H, Ishizaka K, Arima T and Tokura Y 2003 *Nature* **426** 55
- [4] Katsura H, Nagaosa N and Balatsky A V 2005 *Phys. Rev. Lett.* **95** 057205
- [5] Kenzelmann M, Harris A B, Jonas S, Broholm C, Schefer J, Kim S B, Zhang C L, Cheong S W, Vajk O P and Lynn J W 2005 *Phys. Rev. Lett.* **95** 087206
- [6] Mostovoy M 2006 *Phys. Rev. Lett.* **96** 067601
- [7] Sergienko I A and Dagotto E 2006 *Phys. Rev. B* **73** 094434
- [8] Yamasaki Y, Miyasaka S, Kaneko Y, He J-P, Arima T and Tokura Y 2006 *Phys. Rev. Lett.* **96** 207204
- [9] Lawes G, Melot B, Page K, Ederer C, Hayward M A, Proffen T and Seshadri R 2006 *Phys. Rev. B* **74** 024413
- [10] Martinho H, Moreno N O, Sanjurjo J A, Rettori C, García-Adeva A J, Huber D L, Oseroff S B, Ratcliff W, Cheong S.-W, Pagliuso P G, Sarrao J L, and Martins G B 2001 *Phys. Rev. B* **64** 024408
- [11] Sianou A K, Stergioudis G A, Efthimiadis K G, Kalogirou O, and Tsoukalas I A 2005 *J. Alloys Compd.* **392** 310
- [12] Cheong S W and Mostovoy M 2007 *Nature Mater.* **6** 13

- [13] Tackett R, Lawes G, Melot B C, Grossman M, Toberer E S and Seshadri R 2007 *Phy. Rev. B* **76** 024409
- [14] Fritsch V, Hemberger J, Büttgen N, Scheidt E W, Krug von Nidda H A, Loidl A and Tsurkan V 2004 *Phys. Rev. Lett.* **92** 116401
- [15] Büttgen N, Hemberger J, Fritsch V, Krimmel A, Mücksch M, von Nidda H A K, Lunkenheimer P, Fichtl R, Tsurkan V and Loidl A 2004 *New J. Phys.* **6** 191
- [16] Bergman D, Alicea J, Gull E, Trebst S and Balents L 2007 *Nature Phys.* **3** 487
- [17] Blasse G 1963 *Philips Res. Rept.* **18** 383
- [18] Baltzer P K, Lehmann H W and Robbins M 1965 *Phys. Rev. Lett.* **15** 493
- [19] Baltzer P K, Wojtowicz P J, Robbins M and Lopatin E 1966 *Phys. Rev.* **151** 367
- [20] Ramirez A P, Cava R J and Krajewski J 1997 *Nature* **386** 156
- [21] Rudolf T, Kant C, Mayr F, Hemberger J, Tsurkan V and Loidl A 2007 *New J. Phys.* **9** 76
- [22] Ortega-San-Martín L, Williams A J, Gordon C D, Klemme S and Attfield J P 2008 *J. Phys. Cond. Matter* **20** 104238
- [23] Ohgushi K, Okimoto Y, Ogasawara T, Miyasaka S and Tokura Y 2008 *J. Phys. Soc. Jpn.* **77** 034713
- [24] Kino Y and Lüthi B 1971 *Solid State Comm.* **9** 805
- [25] Lee S H, Broholm C, Kim T H, Ratcliff W and Cheong S W 2000 *Phys. Rev. Lett.* **84** 3718
- [26] Tomiyasu K, Fukunaga J and Suzuki H 2004 *Phys. Rev. B* **70** 214434
- [27] Bérar J and Baldinozzi G 1998 *IUCr-CPD Newsletter* **20** 3
- [28] Albuquerque A F et al. 2007 *J. Magn. Magn. Mater.* **310** 1187
- [29] Shannon R D 1976 *Acta Crystallogr. A* **32** 751
- [30] Hill R J, Craig J R and Gibbs G V 1979 *Phys. Chem. Minerals* **4** 317
- [31] Nakatsuka A, Ikeda Y, Nakayama N and Mizota T 2006 *Acta Crystallogr. E* **62**(5) i109
- [32] Cossee P and van Arkel A E 1960 *J. Phys. Chem. Solids* **15** 1
- [33] Yan L Q, Maciá F, Jiang Z W, Shen J, He L H and Wang F W 2008 *J. Phys. Condensed. Matter* **20** 255203
- [34] Blazey K W 1966 *Solid State Comm.* **4** 541
- [35] Mott N F 1972 *Philos. Mag.* **26** 1015
- [36] Mott N F 1981 *Philos. Mag. B* **44** 265
- [37] Ramirez A P and Kowach G R 1998 *Phys. Rev. Lett.* **80** 4903–4906
- [38] Lyons D H, Kaplan T A, Dwight, K and Menyuk N 1962 *Phys Rev* **126** 540
- [39] Ederer C and Komelj M 2007 *Phys Rev B* **76** 064409
- [40] Tomiyasu K and Itoh S 2006 *J. Phys. Soc. Jpn.* **75** 084708